

Conductivity in partially saturated porous media described by porosity, electrolyte saturation and saturation-dependent tortuosity and constriction factor

Carl Fredrik Berg^{1*}, W. David Kennedy² and David C. Herrick³

¹Department of Geoscience and Petroleum, NTNU, S. P. Andersens veg 15, Trondheim, 7031, Norway, ²QED Petrophysics LLC, 14537 Diamondhead North Road, Montgomery, Texas 77354, USA, and ³Yellowstone Petrophysics LLC, 14422 West Hoyt Road, Rathdrum, Idaho 83858, USA

Received August 2020, revision accepted November 2021

ABSTRACT

Modelling the relationships among bulk conductivity, electrolyte conductivity, porosity and fractional electrolyte-saturation continues to be based on empirical relationships such as Archie's law or the Bruggeman correlation. Several authors have attempted to connect such empirical models to first principles. This article presents a complete first principles-based description of conductivity in partially saturated porous media. A geometrical factor is introduced which, together with porosity and saturation, describes the conductivity of partially saturated porous media. This geometrical factor is separated into two intrinsic geometrical descriptors of the electrolyte distribution accounting for tortuosity and constriction. This tortuosity and constriction factor are obtained from integration over the electrical field lines traversing the electrolyte. Bulk and saturation-dependent conductance descriptions are illustrated using three-dimensional pore space models and simulated fluid distributions. Describing conductance through porosity, saturation and a geometrical factor, decomposed into separate terms accounting for tortuosity and constrictivity, permits more insightful understanding of conductance in partially saturated porous media. Use and efficacy of this full conductance description is illustrated throughout this article.

Key words: Petrophysics, Resistivity, Mathematical formulation, Tomography.

INTRODUCTION

Electrical conductance of partially saturated porous media occurs in a wide range of processes and in materials as different as batteries, soils and rocks. Earth science applications include estimation of water saturation in soils or oil and gas content in hydrocarbon reservoirs based on the responses of logging instruments in wells. Air, hydrocarbon gas and oil are almost perfectly insulating compared to the conductivity of the brine. Therefore, the brine is an electrolyte partially saturating the porous medium, while the other fluids and the solid phase con-

tribute negligibly to the overall conductivity. When a partially saturating electrolyte is the main contributor to conductivity, the amount and distribution of the electrolyte are controlling factors for the effective conductivity of porous media.

The description of effective conductivity of a system consisting of several phases with different conductivity can be traced back at least to Maxwell. Assuming conservation of potential and flux on the interfaces, Maxwell described the effective conductivity of a compound medium consisting of spheres with one conductivity inside a substance with another conductivity. However, Maxwell assumed that the distance between the spheres was large compared to their radii so that mutual interactions could be neglected (Maxwell, 1873). When interactions can no longer be neglected, one needs to numerically

*E-mail: carl.f.berg@ntnu.no

solve the electric field to obtain an effective conductance for a given geometry. The exceptions are very simplified geometries which can be solved analytically. Due to such complications, there is a need for theories linking effective conductivity to a few parameters absorbing the complexity of the geometry of the distribution of the conducting phases. Building on results for simplified geometries consisting of spheres or cylinders, Bruggeman obtained effective properties from a method of iteratively embedding two phases into a background material (Bruggeman, 1935). When one of the phases is considered insulating, this led to a description of the effective conductance σ_0 of the conducting phase σ_w as a power law of the volume fraction of the conducting phase ϕ , $\sigma_0 / \sigma_w = \phi^m$. The exponent m was dependent on the geometry of the inclusions, with spheres and cylinders yielding 3/2 and 2, respectively. Although the only parameter in Maxwell's equation was the fractional volume of the two media, Bruggeman's developments led to a power law in the fractional volume, where the exponent depended on the geometry of the conducting phase.

For partially brine-saturated porous media such as soils or hydrocarbon reservoirs, it is common to assume that both the solid phase and the second fluid (gas or oil) are insulating. Following Bruggeman, the effective conductivity could be described by the conductivity and saturation of the conducting phase (brine), in addition to a parameter adsorbing the effect of the geometrical distribution of the conducting phase. Attempts to understand formation conductivity σ_t quantitatively began in the mid-1930s. Between 1936 and 1938, four studies were published (Wyckoff & Botset, 1936; Jakosky & Hopper, 1937; Leverett, 1938; Martin *et al.*, 1938) reporting the relationship between the bulk resistivity $\rho_t = 1/\sigma_t$ of a rock sample to the fractional brine volume S_w in its pore space. The bulk resistivity ρ_t was parameterized as the *resistivity index* $I_R = \rho_t/\rho_0$, dividing the bulk resistivity by the resistivity of a fully brine-saturated sample, $\rho_0 = 1/\sigma_0$. The primary concern of these authors had been the relationship between permeability and porosity. It was left to Archie in 1942 to notice that these authors had independently recorded essentially the same relationship between fractional brine saturation S_w and the resistivity index, namely, a power law: $\rho_t/\rho_0 \equiv S_w^{-n}$. By convention, the *saturation exponent* n is taken to be a positive number, with its value typically approximately equal to 2 (Ellis & Singer, 2007).

In the same paper, Archie introduced the *formation resistivity factor*, F , the ratio of the resistivity $\rho_0 = 1/\sigma_0$ of the brine-saturated sample to the resistivity $\rho_w = 1/\sigma_w$ of the brine in the pore volume, $F = \rho_0 / \rho_w = \sigma_w / \sigma_0$. Archie also

observed that the relationship between the formation resistivity factor and the sample porosity ϕ could be estimated by a power law as $F = \rho_0 / \rho_w \equiv \phi^{-m}$. Note that this is the reciprocal of the Bruggeman relation. Archie observed that m typically was in a range of 1.8–2 for consolidated sandstones (Archie, 1942), thus between the values obtained by Bruggeman for spheres and cylinders.

Combining the two power-laws gives what is commonly referred to as *Archie's law*:

$$\rho_t = a \rho_w \phi^{-m} S_w^{-n}, \quad (1)$$

where it has become customary to include an additional fitting parameter a , first introduced by Owen (1952). The physical interpretations of bulk resistivity ρ_t , brine resistivity ρ_w , porosity ϕ , and water saturation S_w are obvious. Note that as there is no information on the geometrical distribution of the conducting phase in these parameters, thus the electrical effects of the conducting phase geometry must be contained in the remaining parameters m , n and a . There has been a significant effort to attribute physical significance to these parameters, which has led to the commonly used names of *cementation exponent* for m (Guyod, 1944) and *tortuosity factor* for a (Schopper, 1966). However, there is no argument based on physical first principles that links cementation with m , nor tortuosity with a ; these relationships (and corresponding misnomers) are based solely on correlations.

Relating the effective conductance, or similarly, the effective diffusion or hydraulic conductance, to the tortuosity of the porous medium can be traced back at least to Slawinski (1926) and Kozeny (1927). A consensus on the definition of tortuosity has never been reached, partly due to the complexity of most natural porous media (Clenell, 1997). Geometrical definitions relate the length of the medium L to the length of paths through the medium L' , thus $\tau = L'/L$. This tortuosity has been related to the reduction in effective transport; for example, the reduced conductance in a porous medium (Carman, 1937; Wyllie & Rose, 1950; Cornell & Katz, 1953)

$$\frac{\sigma_0}{\sigma_w} = \phi \tau^{-2}. \quad (2)$$

This equation is often used as an empirical definition of tortuosity, due to the lack of both definition and measurement methods to obtain the path length L' .

It was observed that using Equation (2) in low conductivity media to obtain the tortuosity could lead to unrealistically long paths inside the porous medium. Low conductivity could

alternatively be explained by the variation in cross-sectional area along paths (Owen, 1952; Petersen, 1958; Currie, 1960). This effect can be included in Equation (2) as a constriction factor C (Owen, 1952; Van Brakel & Heertjes, 1974):

$$\frac{\sigma_0}{\sigma_w} = \frac{\phi}{\tau^2 C}. \quad (3)$$

There is no consensus on the definition of the constriction factor, and there are no traditional measurement methods to obtain the tortuosity and constriction factor individually. Suggested methods for obtaining the tortuosity and constriction factor include calculations based on pore size distribution curves or directly on images resolving the pore structure (Knackstedt & Zhang, 1994; Koponen *et al.*, 1997; Matyka *et al.*, 2008; Holzer *et al.*, 2013).

Archie did not connect his power laws to pore structure, nor did he predict his relationships through an analysis from first principles; he merely selected power law fits to observed data. It is thus an empirical relationship, as there are no *a priori* physics in the Archie equation. Regardless that Archie's law is merely an empirical model for the rocks in his data set, it is reasonable that it should work for similar rocks. Indeed, for a restricted class of rocks, the Archie law works very well. Rocks where the porosity-conductivity relationship is adequately described by Archie's model are called *Archie rocks* (Herrick, 1988). Such Archie rocks are typically sandstones without a microporous phase (without clays or porous grains) and with a small grain size variation, giving a simple intergranular pore system. Due to its wide applicability and simplicity, the Archie model was quickly and universally adopted, and it remains in use to this day (Ellis & Singer, 2007; Tiab & Donaldson, 2015).

There have been later attempts to derive Archie's law from first principles. It was shown by Sen *et al.* (1981) that Archie's law is consistent with the work of Bruggeman (1935) and later Hanai (1968); however, this result is applicable only to non-conductive particles dispersed in a conductive matrix. For dispersed spheres, the original work of Bruggeman would give $m = 3/2$, which is comparable to experimental results for fused spherical glass beads (Sen *et al.*, 1981). Even though the derivation holds only for dispersed particles, the so-called Bruggeman correlation has been applied to a wide range of materials (Tjaden *et al.*, 2016).

It is thus possible to deduce Archie's law from an effective medium approximation, or mixing rule, for relatively simple porous media. Unfortunately, the models used are hardly representative of rocks. There is therefore no

physical explanation for the parameters used in the Bruggeman or Archie models when applied to complex porous media. Due to the lack of physical basis for the Archie formula, the adjustable parameters have merely been correlated to rock properties. Efforts to characterize the parameters used in the Archie model in terms of rock properties has been ongoing since Archie's work and continue to this day (Glover, 2009; Montaron & Han, 2009; Holzer *et al.*, 2013; Ghanbarian & Berg, 2017; Duy Thanh *et al.*, 2019). Reviews have been conducted by Cai *et al.* (2017) and Ghanbarian *et al.* (2013a).

Even though the Archie model has a proven record of solving problems related to conductivity of rocks, the lack of physical basis and thereby lack of physical interpretation of the adjustable parameters motivates the search for an alternative theory. The formation factor has been described by first principles, where the effective conductivity is formulated as an integral of the pore space of the microscopic electrical potential (Johnson *et al.*, 1986). Johnson *et al.* used this pore scale integral formulation to define a characteristic pore size, thereby linking conductance to permeability. Later, Pride (1994) derived macroscopic governing equations controlling the coupled electromagnetics and acoustics in porous materials from first principles. Pride used the work of Johnson *et al.* (1986) to describe the geometry of the pore structure and a characteristic pore size. To be classified as Archie rocks, there must be negligible surface conductivity relative to the conductivity of the electrolyte. A popular modification of Archie's model for including surface conductance is the Waxman-Smits model (Waxman & Smits, 1968). The models of Johnson *et al.* (1986) and Pride (1994) have been extended to include surface conductance by Revil and Glover (1997).

An effective conductivity formulation similar to Johnson *et al.* (1986) was independently proposed by Herrick and Kennedy (1994). Further, by extending the results to fractional brine saturations, they formulated a complete alternative theory to Archie's law. Herrick and Kennedy (2009) call this model the geometrical factor theory; it is restated in this article for completeness.

The physical explanation for the parameters in the theory proposed herein is alluded to in the original paper by Herrick and Kennedy (1994), where it was substantiated that the geometrical factor represented the tortuosity and constrictions of the pore structure. This physical explanation was confirmed by Berg (2012) for fully saturated porous media. In that article, Berg integrated infinitesimal elements of conducting brine volume elements into tortuosity and constriction factors, and

the combined effect of the tortuosity and constriction factor gives the geometrical factor. Berg's model provides a complete theory for electrical conductivity in saturated rocks based on first principles, where the parameters are firmly linked to the pore structure of the rock. In this article, we will extend this theory to partially saturated porous media.

THE GEOMETRICAL FACTOR THEORY

A reservoir rock can be considered as comprising a conductive phase (brine) and possibly several non-conductive phases. The non-conductive phase is typically the matrix of the rock; for example, quartz grains, and, if present, also non-conductive fluids such as oil and/or gas that partially fill the pore-space of the rock. The conductive phase is primarily an electrolyte (brine). Reservoir rocks often contain other conductive phases, such as mineral surfaces, clays and metallic sulphides, commonly pyrite. For simplicity, we will assume a single conductive phase, that is, a brine filling (or partially filling) the pore space, with constant conductivity σ_w . We will thus exclude surface conductance and clays from our analysis. It should be noted that these effects can be included into our theories if a thin but finite thickness conductor is applied to the grain surfaces.

Consider a rock sample of volume V consisting of an insulating matrix and possibly an insulating fluid partially filling the pore volume, together with an electrolyte (brine) filling the remaining pore volume Ω in the model. The sample has a length L in direction of an applied potential difference $\Delta\Phi$ over the side planes, and the sample has a constant cross-sectional area A . The constant voltage drop $\Delta\Phi$ leads to a direct current. For illustration purposes, we have created a two-dimensional model resembling a rock sample. A cross-section of an actual rock sample has little or no through-going connectivity and can therefore not be used for two-dimensional numerical modelling of current flow. Thus, if a model with realistic-looking grains is desired, the grains from a rock image must be separated in order to provide a path for the currents to be modelled. Figure 1 is a two-dimensional model based on a cross-section of a rock sample, where we have eroded the matrix significantly to increase the connectedness in this two-dimensional plane.

Inside the electrolyte, the current density \mathbf{J} is given by Ohm's law as $\mathbf{J} = \sigma_w \mathbf{E}$, where \mathbf{E} is the electrostatic field. The electrostatic field $\mathbf{E} = -\nabla\Phi$ is given by the gradient of the electrical potential Φ . The change of electric charge in any volume equals the amount of charge flowing into the volume minus the amount of charge flowing out. For a given point,

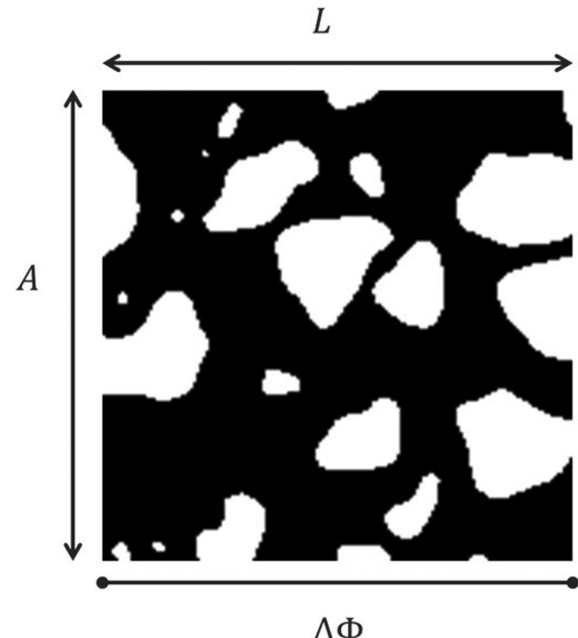


Figure 1 A 2D cross-section resembling a rock sample, with a fully electrolyte-saturated pore space Ω in black and rock matrix in white. The sample has length L with a potential difference of $\Delta\Phi$ applied between the vertical sides of the sample. This 2D model is based on a rock sample; however, the irregular grains have been separated from each other to permit through-going continuity of the conductive fluid phase required to illustrate conduction in a 2D model.

the change of electric charge is given by the divergence of the current density $\nabla \cdot \mathbf{J}$. At steady state, we then have $\nabla \cdot \mathbf{J} = 0$. Combining the equations above implies that the electrical potential must satisfy the Laplace equation

$$\nabla \cdot \mathbf{J} = \nabla \cdot \sigma_w \mathbf{E} = -\nabla \cdot \sigma_w \nabla\Phi = -\sigma_w \nabla^2\Phi = 0, \quad (4)$$

with the boundary condition $\Phi = \Phi_{\text{in}}$ on the left and $\Phi = \Phi_{\text{out}}$ on the right, and where the electrolyte conductivity σ_w is constant. Electric current cannot flow into or out of any non-conductive phase, therefore the current must flow parallel to the interface between the conductive phase (brine) and the non-conductive phase (matrix); that is, parallel to the grain surfaces since no current can flow into or out of the non-conductive grains.

Consider now the power developed in the conducting phase. The total power developed is given by

$$P = \int_{\Omega} \mathbf{J} \cdot \mathbf{E} dV = \int_{\Omega} \sigma_w \nabla\Phi \cdot \nabla\Phi dV = \int_{\Omega} \sigma_w \|\nabla\Phi\|^2 dV. \quad (5)$$

At the same time, the total power is given by the product of total current I and applied voltage drop $\Delta\Phi$. This gives the following expression for the total current:

$$I = \frac{1}{\Delta\Phi} \int_{\Omega} \sigma_w \|\nabla\Phi\|^2 dV. \quad (6)$$

By definition, the effective conductivity, σ_t , of our sample is

$$\sigma_t = \frac{\left(\frac{I}{A}\right)}{\left(\frac{\Delta\Phi}{L}\right)} = \frac{IL}{A\Delta\Phi}. \quad (7)$$

Dividing Equation (7) by σ_w and substituting I from Equation (6) gives

$$\frac{\sigma_t}{\sigma_w} = \frac{IL}{\sigma_w \Delta\Phi A} = \frac{L}{A\Delta\Phi^2} \int_{\Omega} \|\nabla\Phi\|^2 dV, \quad (8)$$

thus expressing the conductivity of the medium as an integral over the electrolyte volume. By manipulating the equation, we can write it in the following form

$$\frac{\sigma_t}{\sigma_w} = \phi S_w \frac{1}{\Omega} \int_{\Omega} \frac{\|\nabla\Phi\|^2}{\Delta\Phi/L^2} dV = \phi S_w E_t, \quad (9)$$

where we have expressed the conductivity by the fractional amount of electrolyte as given by ϕS_w and an integral over the electrolyte volume linked to the local gradient in the electric field. Here we have denoted the integral $(1/\Omega) \int_{\Omega} \nabla\Phi^2 / \Delta\Phi/L^2 dV$ as E_t . (For a detailed derivation of Equation (9), see Appendix A.) We can express Equation (9) similarly to Archie's model (Equation (1)) as $\rho_t = \phi^{-1} S_w^{-1} E_t^{-1} \rho_w$, or reciprocally as $\sigma_t = \phi S_w E_t \sigma_w$. Assuming a fully water-saturated sample, $S_w = 1$, we then have $\sigma_t = \sigma_0$, and get the following expression for the *formation conductivity factor* f :

$$f = F^{-1} = \frac{\rho_w}{\rho_0} = \frac{\sigma_0}{\sigma_w} = \phi E_0. \quad (10)$$

Following Kennedy and Herrick (2012), we define E_t and E_0 as *geometrical factors* which account for the reduction in conductivity due to the geometric distribution of the non-conductive phase. Thus, the geometrical factor is deduced from first principles, and it is the building block of the geometrical factor theory presented in Kennedy and Herrick (2012). It should be noted that E_t is called *electrical efficiency* by Herrick and Kennedy (1994) and *conductance reduction factor* by Berg (2012).

PORE STRUCTURE DESCRIPTION OF THE GEOMETRICAL FACTOR

The geometrical factor E_0 , and likewise E_t , are dependent on electrolyte geometry and have no intrinsic relationship to porosity. In this section, we will link the geometrical factor to geometrical descriptors, namely the tortuosity and constriction factor. We begin with motivating examples on simplified pore geometries, before treating a general complex pore structure.

Tortuosity

One well-known geometrical descriptor is the tortuosity (Clennell, 1997; Ghanbarian *et al.*, 2013a). In Fig. 2(a), we have visualized the direction of the electric field $\mathbf{E} = -\nabla\Phi$. An electric field line is a line from the inlet to the outlet that is always parallel to the electric field, as visualized in Fig. 2(b). The actual length L_{Γ} of an electric field line Γ inside the pores of our rock sample is longer than the length of the rock sample L . In other words, the electric field line is tortuous, and the magnitude is described by the *tortuosity* $\tau(\Gamma) = L_{\Gamma}/L$ of the field line Γ . As the electric field line is always longer or equal to the length of the sample, the tortuosity is a number greater than or equal to 1. A larger tortuosity value indicates a more tortuous (i.e. longer) electric field line. Note that there is no consensus on how tortuosity should be defined; see Clennell (1997) for an overview. Other common definitions include $(L_{\Gamma}/L)^2$ (see Wyllie & Rose, 1950), and the reciprocal definition L/L_{Γ} (see Bear (1988) or Berg (2012)).

Following Dullien (1992) and Pfannkuch (1972), consider a single cylindrical tube of length L' as depicted in Fig. 3. Disregarding that the field lines will have a slightly different geometry than the geometry of the tube, the length of the field lines L_{Γ} can be approximated as the tube length L' . The volume of the tube will be *larger* than a similar tube with equal cross-sectional area of length L by a factor $\tau = L'/L$. The applied potential $\Delta\Phi$ divided by the length of the field lines $L_{\Gamma} \simeq L'$ gives the magnitude of the electric field $\|\mathbf{E}'\| = \Delta\Phi/L'$ along the field lines. In this tube, the local current density $\|\mathbf{J}'\| = \sigma_w \|\mathbf{E}'\| = \sigma_w \Delta\Phi/L'$ will be *smaller* by a factor $1/\tau = 1/(L/L') = L'/L$ than in a straight tube of length L where the local current density would be $\|\mathbf{J}\| = \sigma_w \Delta\Phi/L$. So, the tortuous tube has increased the volume and at the same time decreased the conductance by the same factor (i.e. $1/\tau = L/L'$) compared to a (straight) tube of equal radius but length L . A straight tube would give the bulk medium an effective conductivity given by the brine conductivity reduced by the

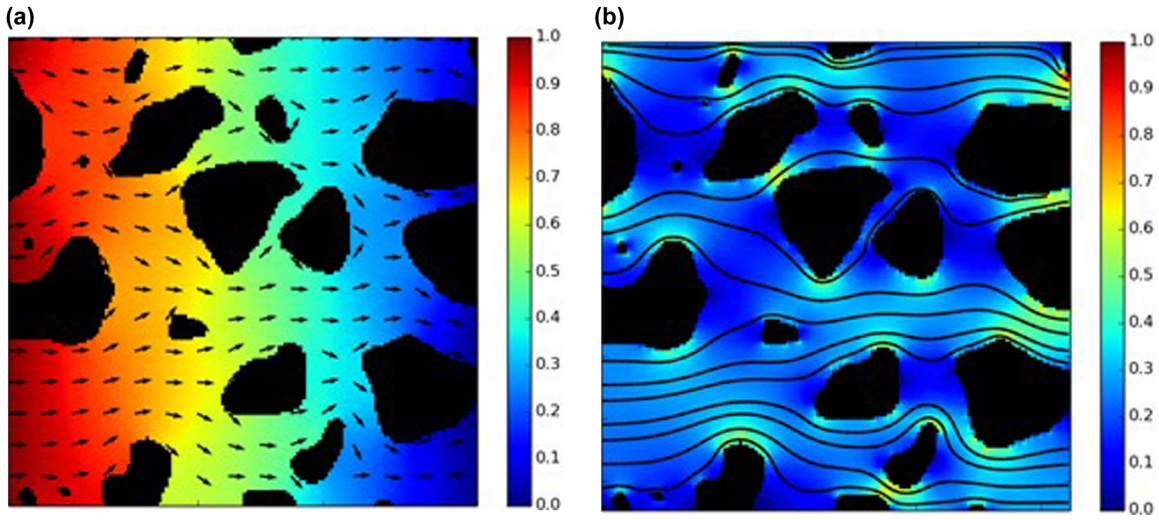


Figure 2 A potential difference is applied to the model shown in Fig. 1. (a) Arrows indicating the direction of the electric field $E = -\nabla\Phi$, where the colours show the underlying electrical potential Φ . The potential is 1 on the left and 0 on the right. (b) Lines indicating selected members of the set of electric field lines through the pore space, where the background colours represent the normalized magnitude of the electrostatic field $E = \nabla\Phi$.

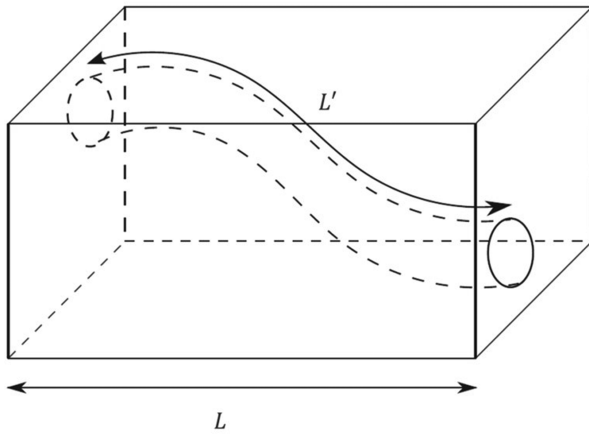


Figure 3 An idealized porous medium consisting of a single tortuous tube of length L' inside a box of side-length L .

porosity; that is, $\sigma_0 = \phi\sigma_w$. For a tortuous tube, the combined effects of the volume increase ($1/\tau$) and the conductance decrease (also $1/\tau$) act together to decrease the effective conductivity of the medium, yielding the effective conductivity as

$$\sigma_0 = \sigma_w \phi \tau^{-2}. \quad (11)$$

The correspondence between the length of the field lines and the interstitial current was first noted by Kozeny in the context of fluid flow (Kozeny, 1927). Building on the work of Kozeny, Carman (1937) noted that the magnitude of the average interstitial current density J_x in direction x of the applied po-

tential equals $\|J_0\|/\phi$, where $\|J_0\| = \sigma_0 \Delta\Phi/L$ is the effective current density for the porous medium and σ_0 is the effective conductivity of the bulk medium (Carman, 1937). The interstitial current density $\|J\|$ is related to the average interstitial current density in the direction of the applied potential $\|J\|_x$ by a factor of $\tau = L_\Gamma/L$, thus the average interstitial current density $\|J\| = \sigma_w \Delta\Phi/L_\Gamma$ equals $\|J\|_x \tau = (\|J\|_0/\phi) (L_\Gamma/L) = (\sigma_0/\phi) (\Delta\Phi/L) (L_\Gamma/L)$. By rearranging the terms in $\|J\| = \|J\|_x \tau$, this reduces to the Kozeny–Carman equation reformulated to electrical conductivity as given by Equation (11) above (see Appendix B for a more detailed derivation).

Visual inspection of Fig. 2(b) reveals that in this simplified two-dimensional example the tortuosities for the streamlines are not much larger than 1. Carman (1937) reported observing $\tau = \sqrt{2}$ for glass spheres. It can be shown that for a cubic sphere pack the maximum tortuosity is approximately $\pi/2$. For simple granular porous media, the tortuosity is often in the same range as for the sphere pack; that is, in the range 1–2. However, there are rocks that have higher tortuosity values, for example, highly cemented sandstones or sandstones with large amounts of mica.

The model of Kozeny–Carman is in effect a bundle of capillary tubes and has repeatedly been modelled as such (Dullien, 1992). This includes models with fractal distribution of capillary sizes (Wheatcraft & Tyler, 1988; Yu & Cheng, 2002; Duy Thanh *et al.*, 2019; Rembert *et al.*, 2020) based on fractal dimensions of pore size distributions (Katz & Thompson, 1985). Network models, as pioneered by Fatt (1956), is

another extension of the bundle of capillary tubes, enabling tortuosity calculations for more realistic models of porous media (Dullien, 1992). Network models have for a long time identified why the tortuosity is insufficient to fully describe conductance, as they do not account for constrictions in the porous medium (Schopper, 1966; Dullien, 1975). This will be treated in the next section.

Constriction factor

The geometrical factor theory introduced in Section 2 asserts $\sigma_0 = \sigma_w \phi E_0$ (Equation 10). From Equation (11), this would imply $E_0 = \tau^{-2}$. Measurements on core samples show that the geometrical factor E_0 approaches zero for low porosities (see, for example, Fig. 6). The tortuosity τ cannot approach infinity for low porosities, as this would indicate that electric field lines are approaching infinite length, which is impossible as the electric field is smooth and the porous medium is finite. Thus, it follows that the geometrical factor E_0 must be controlled by more than the tortuosity alone.

An additional factor was pointed out by Owen (1952); the constricting nature of porous media limits the current flow. For sandstones, the pore space can be loosely divided into pore bodies being the larger space between the grains, while the narrower spaces connecting the pore bodies are called pore throats. The current will then sequentially pass through pore bodies and pore throats. As the conductance is proportional to the cross-sectional area, the variation in cross-sectional area between the pore bodies and pore throats will limit the current (Owen, 1952; Petersen, 1958; Currie, 1960; Dullien, 1992). It is typically more pronounced in three dimensions than in two that the magnitude of the electric field is larger in the pore throats than in the pore bodies. Still, this can be observed in Fig. 2(b); close to the right boundary, the cross-section contains more of the non-conductive matrix, thus there is less of the conductive phase and the magnitude of the electric field becomes larger.

Following Dullien (1992) and Petersen (1958), a return to a simple pore volume model is instructive; we now consider a prism with a single embedded electrolyte-filled cylindrical tube with varying cross-sectional area of $A(x)$ at a distance x along the tube of total length L , as illustrated in Fig. 4. In this example, we will assume that the length L is much larger than the variation in cross-sectional radii, so that the length of the electric field lines L_Γ will be approximately equal the length of the porous medium, that is, $L_\Gamma \simeq L$. Although small, there will always be a contribution from tortuosity in such a constriction example (as there will always be a small contribution

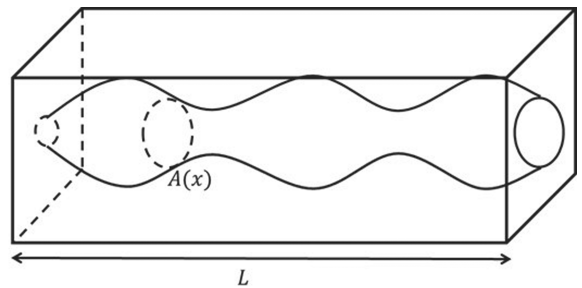


Figure 4 An idealized porous medium consisting of a single brine-filled tube of varying cross-sectional area $A(x)$ inside a cube of side-length L .

from constriction in an idealized tortuosity example as the one illustrated in Fig. 3).

If the pore channel in Fig. 4 had constant radius, then the conductivity of the prism would be $\sigma_0 = \sigma_w \phi$. Or, in resistivity terms, $\rho_0 = \rho_w \phi^{-1}$. When the pore channel radius has constrictions, the effective conductivity of the prism diminishes; equivalently, its effective resistivity increases. This is parameterized as $\rho_0 = C \rho_w \phi^{-1}$ where C expresses the increase in resistivity. The resistance of a thin disk centred on the cross-sectional area at x , $dR_t(x)$ will be proportional to brine resistivity, ρ_w , the thickness of the disk, dx , and inversely proportional to the area of the disk, $1/A(x)$. Thus $dR_t(x) = \rho_w (1/A(x))dx$. Assuming that the equipotential surfaces for the electric field are everywhere flat and perpendicular to the direction x , in other words neglecting any contribution from tortuosity, the total resistance along the tube is the integral of the local resistance:

$$R_t = \int_0^L dR_t(x) = \rho_w \int_0^L \frac{1}{A(x)} dx, \quad (12)$$

where R_t is the cumulative resistance over the tube, and L is the length of the tube. The smallest pore throats have the highest resistance and tend to dominate the integral. A tube of equal length and resistance, but with constant cross-sectional area would then have an effective cross-sectional area of A_e given by

$$A_e = \frac{L}{\int_0^L \frac{1}{A(x)} dx}. \quad (13)$$

The effective area A_e is always smaller than, or at most equal to, the average cross-sectional area, $\bar{A} = \int A(x)dx/L$, of a tube with varying cross-sectional area. Thus, the pore volume of a tube with same resistance and constant cross-sectional area is less than the pore volume of the tube with variable

cross-sectional area. Following Owen (1952), the ratio of these areas is denoted the *constriction factor* C :

$$C = \frac{\bar{A}}{A_e} = \frac{1}{L} \int A(x) dx \frac{1}{L} \int \frac{1}{A(x)} dx. \quad (14)$$

Thus have we found a means to compute C in the resistivity relationship $\rho_0 = C \rho_w \phi^{-1}$. Recasting the relationship into conductivity terms, the single-tube example becomes $\sigma_0 = \sigma_w \phi/C$; thus, we have $E_0 = 1/C$.

From our assumption that the equipotential surfaces are perpendicular to the direction x , the current density \mathbf{J} is constant in any cross-section $A(x)$. As the total current is constant, the current density must be proportional to the inverse of the cross-sectional area, $\|\mathbf{J}(x)\| \propto 1/A(x)$. With a constant electrolyte conductivity, we then have $A(x) \propto -1/\|\mathbf{E}(x)\|$, where $\mathbf{E}(x)$ is the electrostatic field at distance x . We can then reformulate Equation (14) in terms of the electrostatic field:

$$C = \frac{1}{L^2} \int \|\mathbf{E}(x)\| dx \int \frac{1}{\|\mathbf{E}(x)\|} dx. \quad (15)$$

As the cross-sectional area of pore throats are smaller than the cross-sectional area of pore bodies, the equation for the constriction factor C above reveals that the resistance is dominated by the smallest, or current limiting, pore throats. As the cross-sectional areas of the smallest pore throats dominate the integral where the cross-sectional area is in the denominator ($\int 1/A(x)dx$), the smallest pore throats are the limiting factor for the conductivity.

If we want to consider the effects of tortuosity and constrictions acting together, then the product of the expressions for tortuosity and the constriction factor provides an estimate of the conductivity as $\sigma_0 = \sigma_w \phi \tau^{-2} C^{-1}$ (Winsauer *et al.*, 1952; Boyack & Giddings, 1963), which requires $E_0 = \tau^{-2} C^{-1}$. For simplified porous media, it is possible to separate the pore geometry factor E_0 into the independent values of tortuosity and constriction factor. However, as pointed out by Wyllie in a discussion that follows Owens' (1952) article, Winsauer *et al.* failed to resolve the fundamental difficulty of separating these quantities for realistic pore structures.

Effective pore structure parameters

In this subsection, we will generalize the idealized tortuosity and constriction models considered in the two previous subsections, and obtain a description for tortuosity and constriction factor for any type of complex porous medium. Note that the pore space, and thereby the electrolyte, is assumed connected, in the sense that for any point in the pore space there are connected paths fully inside the pore space to the two

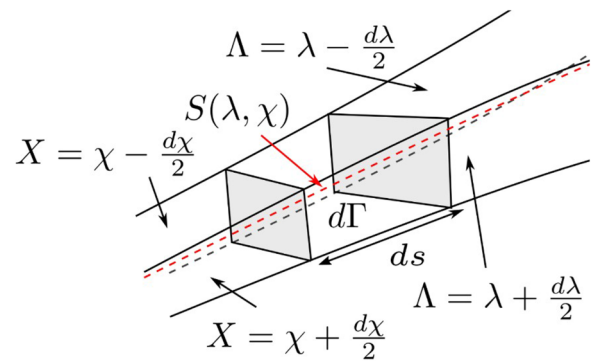


Figure 5 A schematic indicating a portion of a single stream tube. The red dashed line indicates the streamline $S(\lambda, \chi)$. The upper surface is defined by $\Lambda = \lambda - d\lambda/2$, the lower surface is defined by $\Lambda = \lambda + d\lambda/2$, while the left and right surfaces are given by $X = \chi - d\chi/2$ and $X = \chi + d\chi/2$, respectively. The infinitesimal streamtube bounded by the four surfaces has a volume $d\Gamma$, and the streamtube has a constant current dI_Γ .

sides of the porous medium where the potential difference is applied.

For developing general expressions for the tortuosity and constriction factor, we need a mathematical description of the electrical field lines. Following Bear (1988), there exist functions $\Lambda(x, y, z)$ and $X(x, y, z)$ such that the electric field lines are given by intersections of the two surfaces $\Lambda = \lambda$ and $X = \chi$ for constants λ and χ , as illustrated in Fig. 5. That is, the normal vectors of the two surfaces $\Lambda = \lambda$ and $X = \chi$ are both perpendicular to the direction of the electric field $\mathbf{E} = -\nabla\Phi$. Further, the functions Λ and X can be chosen such that for the surfaces given by λ and χ , we have $\nabla\lambda \times \nabla\chi = -\nabla\Phi$. Any field line is then given by the intersection of the surfaces given by a set of constants λ and χ . Thus, any field line S is described by a pair of constants (λ, χ) , where $S(\lambda, \chi)$ is the intersection of the two surfaces given by $\Lambda = \lambda$ and $X = \chi$. Together with a parameter s describing the distance along a streamline, the three coordinates (λ, χ, s) describe all points in the pore space (electrolyte).

Transforming from Cartesian coordinates (x, y, z) to the field line coordinates (λ, χ, s) , we need to multiply by the Jacobian J (not to be confused with the current density \mathbf{J} using a similar notation):

$$J = \nabla s \cdot \nabla\lambda \times \nabla\chi = \begin{vmatrix} \frac{\partial s}{\partial x} & \frac{\partial s}{\partial y} & \frac{\partial s}{\partial z} \\ \frac{\partial \lambda}{\partial x} & \frac{\partial \lambda}{\partial y} & \frac{\partial \lambda}{\partial z} \\ \frac{\partial \chi}{\partial x} & \frac{\partial \chi}{\partial y} & \frac{\partial \chi}{\partial z} \end{vmatrix}. \quad (16)$$

The last term denotes the determinant. As the direction of s is given by the electric field $\mathbf{E} = -\nabla\Phi$, we have $\nabla s = -\nabla\Phi/\|\nabla\Phi\|$. We then get the Jacobian as

$$J = \nabla s \cdot \nabla \lambda \times \nabla \chi = \frac{\nabla \Phi}{\|\nabla \Phi\|} \cdot \nabla \Phi = \frac{\|\nabla \Phi\|^2}{\|\nabla \Phi\|} = \|\nabla \Phi\|. \quad (17)$$

We can then do a coordinate transformation from Cartesian coordinates to field line coordinates as

$$\int_{\Omega} dV = \int \int \int dx dy dz = \int \int \int_{S(\lambda, \chi)} \frac{1}{\|\nabla \Phi\|} ds d\lambda d\chi, \quad (18)$$

where $\Omega \subset \mathbb{R}^3$ is a subspace, in our case representing the volume occupied by the electrolyte. Alternatively, for saturated samples the subspace Ω would represent the pore space. The infinitesimals $d\lambda d\chi$ give the infinitesimal area around a field line in two directions, thus this gives an infinitesimal streamtube around the field line $S(\lambda, \chi)$ given by the surfaces $\Lambda = \lambda$ and $X = \chi$, as illustrated in Fig. 5. We then get the volume of the infinitesimal streamtube around the field line as

$$\int_{S(\lambda, \chi)} \frac{1}{\|\nabla \Phi\|} ds d\lambda d\chi = d\Gamma, \quad (19)$$

where $d\Gamma$ is the volume of the infinitesimal streamtube around the field line $S(\lambda, \chi)$ as indicated in Fig. 5. Note that the surfaces given by any $\Lambda = \lambda$ or $X = \chi$ are perpendicular to the electric field, therefore the current inside a streamtube is constant for any cross-section of the streamtube. Since $\nabla \lambda \times \nabla \chi = -\nabla \Phi$, we have that $dI_{\Gamma} = \sigma_w d\lambda d\chi$. That is, the infinitesimal current carried by the streamtube given by $d\lambda d\chi$.

Let P be the set of all electric field lines Γ in traversing the electrolyte volume Ω . An effective tortuosity for the porous medium can then be defined as

$$\tau^2 = \left(\frac{1}{\Omega} \int_{\Gamma \in P} \frac{1}{\tau(\Gamma)^2} d\Gamma \right)^{-1}, \quad (20)$$

where $d\Gamma$ is the infinitesimal volume associated with the electric field line Γ (Berg, 2012). The tortuosity has a minimum value of 1, which is reached when all electric field lines are straight and have a length equal to the length of the porous medium. Longer electric field lines give a higher tortuosity, which reduces the efficiency of the electrolyte to conduct electricity. Note that neither the value for the conductivity σ_w of the electrolyte, nor the applied voltage drop $\Delta\Phi$, affects the tortuosity, thus the tortuosity is only dependent on the geometrical structure of the electrolyte volume

and the direction of the applied electric field. Any dependence on the direction of the applied electric field results from anisotropy of the geometrical structure of the electrolyte. This indicates that properties such as tortuosity and constriction are, in fact, tensors. In this article, we only consider properties in one direction. This can be extended to directional properties for anisotropic geometries (Kennedy *et al.*, 2001).

When the electric current passes through a constriction, the current density J is increased. Variation in pore size thus translates into a variation in current density. For a given electrolyte volume, more energy is expended driving a current when the current density varies compared to a case with constant current density, thus the conductive efficiency is reduced with larger variation in current density.

We define the constriction factor $C(\Gamma)$ for an electric field line Γ of length L_{Γ} , similarly to the definition for a single tube in the previous subsection (Equation 15), as

$$C(\Gamma) = \frac{1}{L_{\Gamma}^2} \int_{\Gamma} \|\mathbf{E}(s)\| ds \int_{\Gamma} \frac{1}{\|\mathbf{E}(s)\|} ds = \frac{1}{L_{\Gamma}^2} \Delta\Phi \int_{\Gamma} \frac{1}{\|\mathbf{E}(s)\|} ds, \quad (21)$$

where ds is the infinitesimal arc length along the streamline Γ . The constriction factor C for the electrolyte volume Ω is then the current-weighted average of the constriction factors for the electric field lines,

$$C = \frac{1}{I} \int_{\Gamma \in P} C(\Gamma) dI_{\Gamma}, \quad (22)$$

where I is total current through the electrolyte, and dI_{Γ} is the infinitesimal current associated with the electric field line Γ .

The constriction factor has a minimum value of 1, reached when the electrostatic field is constant along each field line; for example, for a straight tube and approximately for the tube depicted in Fig. 3. Larger variation in the electrostatic field due to changes in the pore's cross-sectional area increases the constriction factor, and thereby reduces the conductivity of the fully saturated porous medium. As with the tortuosity, the constriction factor is solely dependent on the geometrical structure of the electrolyte and the direction of the voltage drop. Note that both the tortuosity and the constriction factor are scale invariant, in the sense that a uniform scaling of the electrolyte geometry (i.e. enlarging or shrinking the whole medium by the same factor in all directions) will not change the tortuosity or the constriction factor.

Combining the field line integrals for tortuosity and constriction factor as given by Equations (20) and (22), and using the Jacobian, Equation (17), to go from a volume integral to

a field line integral, we obtain (see Berg (2012) for a more thorough derivation):

$$\begin{aligned} \frac{1}{\tau^2 C} &= \frac{\frac{1}{\Omega} \int_{\Gamma \in P} \frac{1}{\tau(\Gamma)^2} d\Gamma}{\frac{1}{I} \int_{\Gamma \in P} C(\Gamma) dI_\Gamma} = \frac{I}{\Omega} \frac{\int \int \int_{S(\lambda, \chi)} \frac{L_\Gamma^2}{L_\Gamma^2} \frac{1}{\|\mathbf{E}(s)\|} ds d\lambda d\chi}{\int \int \int_{S(\lambda, \chi)} \frac{1}{L_\Gamma^2} \Delta \Phi \frac{1}{\|\mathbf{E}(s)\|} \sigma_w ds d\lambda d\chi} \\ &= \frac{IL^2}{\Omega \sigma_w \Delta \Phi} = E_0. \end{aligned} \quad (23)$$

For the last equality, we have used Equation (10). This gives an exact expression for our geometrical factor in terms of descriptors of the geometrical structure of the pore space. Rearranging the terms, we then have:

$$E_0 = \tau^{-2} C^{-1}. \quad (24)$$

This expression holds in general, and not only for the simplified pore structures used as motivating examples in the previous two subsections. Thus, the geometrical factor E_0 can be separated into individual contributions from tortuosity and constriction.

PARTIALLY SATURATED POROUS MEDIA

Now consider a rock partially filled with brine; that is, $S_w < 1$. In Equation (9) above, we have $\sigma_t = \sigma_w \phi S_w E_t$, where ϕS_w is the fractional brine volume conducting electricity. In the conductivity representation of Archie's law, $\sigma_t = \alpha^{-1} \sigma_w \phi^m S_w^n$, both the porosity and saturation are raised to a power. In this form, a weakness of the Archie formulation is apparent: the fractional brine volume ϕS_w in the rock has its own unique geometry, and logically it should be treated as a single entity. However, ϕS_w is not treated as a single entity in the Archie model; the factors are treated separately as the result of having been put together from two separate experiments, one using water saturation at fixed porosity and the other using porosity at a fixed water saturation (i.e. $S_w = 1$).

Following the usual convention, we distinguish the geometrical factor E_0 for the fully saturated rock from the geometrical factor E_t for the partially saturated rock. To isolate the modification of the electrolyte geometry due to partial saturation, we normalize the geometrical factor of the partially saturated porous medium by dividing by the geometrical factor of the fully saturated porous medium. The quotient, called the *efficiency index* and denoted $e_i = E_t / E_0$, is then a factor describing the distribution of electrolyte that shares the pore space with non-conductive fluids. Note that the same parameter is denoted e_i by Herrick and Kennedy (2009). The reason for changing the notation in this article is to have the efficiency

index notation in line with its constituent tortuosity and constriction indices (as they occur later in Equations 27 and 28).

Replacing E_t by the components $E_0 e_i$, we get the equation

$$\sigma_t = \phi S_w E_t \sigma_w = (\phi S_w) (E_0 e_i) \sigma_w. \quad (25)$$

The parentheses are added to indicate the fractional volume of the electrolyte and the geometrical factor of the electrolyte. We can rearrange the terms in Equation (25) to highlight the change in conductance relative to the fully saturated medium as

$$\sigma_t = (\phi E_0) (S_w e_i) \sigma_w = \sigma_0 S_w e_i, \quad (26)$$

where S_w gives the reduction in electrolyte volume, while e_i gives the relative change in the geometrical factor. This expression follows the logic of the classical Archie equation; that is, the product of a function of porosity and a function of water saturation. Then the factor e_i should correlate to electrolyte saturation S_w ; as electrolyte is displaced by a non-conductive phase, the electrolyte geometry and thereby e_i changes. Combining this equation with Equations (10), the conductivity of the fully saturated sample is given by $\sigma_t|_{S_w=1} \equiv \sigma_0 = \sigma_w \phi E_0 = \sigma_w \phi \tau^{-2} C^{-1}$.

As explained above, equivalent to the description of E_0 the efficiency E_t can be described by electrolyte geometrical distribution parameters as $E_t = \tau_t^{-2} C_t^{-1}$, where we use subscript t to indicate that the electrolyte distribution parameters are for the partially saturated case. The saturated part of the pore space is then treated identically to the total pore space analysis for the geometric factor E_0 . As the electrolyte-filled part of the pore space changes its shape and distribution in the pore volume with the saturation, the electrolyte distribution parameters also change with the saturation. Note that the distribution of electrolyte is not solely a function of saturation (e.g. hysteresis is ignored); however, it is common to treat the fluid distribution as a function of its saturation. This translates into describing the geometric factor E_t as a function of the volume fraction of the electrolyte: $E_t(\phi S_w)$. As the porosity ϕ is considered constant, this is reduced to considering the geometric factor of a partially saturated rock E_t as a function of the electrolyte saturation $E_t(S_w)$. Equivalently, the electrolyte distribution descriptors are described as functions of saturation as $\tau_t(S_w)$ and $C_t(S_w)$. Note that hysteresis, the process where a formation property depends not only on the electrolyte saturation value but whether it is changing by imbibition or drainage, leads to different fluid distributions at equal saturations. This is treated by considering different efficiencies for drainage and imbibition situations.

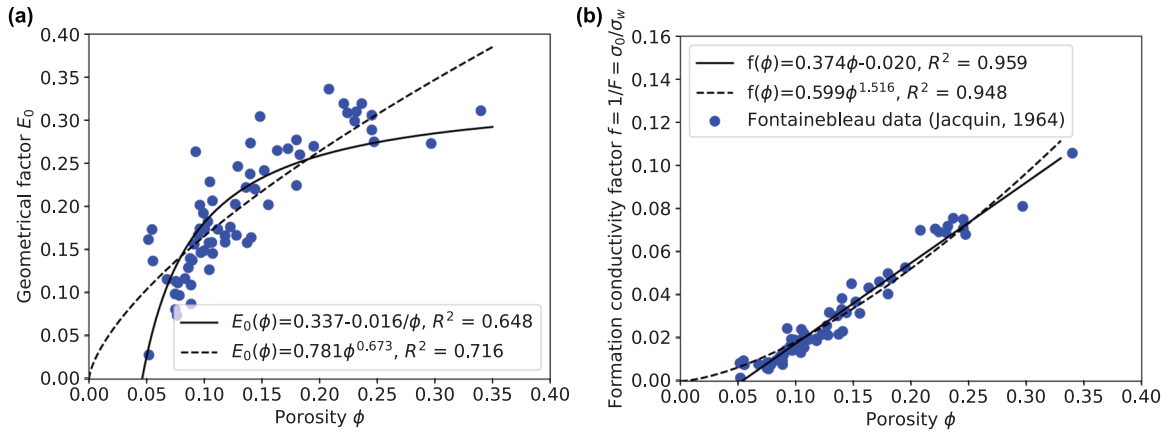


Figure 6 (a) Plot showing the geometrical factor versus porosity for the data from Jacquin (1964). (b) Plot of porosity versus the formation conductivity factor f , together with a linear fit to the data.

To keep the notation separate, we will use the subscript 0 for the fully saturated sample, so that $E_0 = \tau_0^{-2} C_0^{-1}$. As described above, we use the notation $E_t(S_w) = \tau_t^{-2}(S_w)C_t^{-1}(S_w)$ for the partially saturated case. We now want to describe the efficiency index as

$$e_i = \frac{E_t}{E_0} = \frac{\tau_t^{-2}C_t^{-1}}{\tau_0^{-2}C_0^{-1}} = \left(\frac{\tau_t^{-2}}{\tau_0^{-2}} \right) \left(\frac{C_t^{-1}}{C_0^{-1}} \right) = \tau_i^{-2}C_i^{-1}. \quad (27)$$

Here we call $\tau_i = \tau_t / \tau_0$ the tortuosity index, and $C_i = C_t / C_0$ the constriction factor index. These are both functions of saturation, so we can write $e_i(S_w) = \tau_i^{-2}(S_w)C_i^{-1}(S_w)$.

The resistivity index is typically defined as the resistivity at a given saturation divided by the resistivity for a completely saturated sample:

$$I_R(S_w) = \frac{\rho_t(S_w)}{\rho_0} = \frac{\sigma_0}{\sigma_t(S_w)} = \frac{\sigma_0}{\sigma_0 S_w e_i} = \frac{1}{S_w e_i} = \frac{C_i \tau_i^2}{S_w}. \quad (28)$$

This equation shows how the resistivity index depends on the changes in the electrolyte distribution parameters and the saturation. We will apply this resistivity index formulation for rock samples in Section 6.

GEOMETRICAL FACTOR FOR SANDSTONES

This section illustrates the geometrical factor theory described in Section 2 by applying it to a set of sandstones samples. We will consider a set of Fontainebleau sandstone data investigated by Jacquin (1964). The Fontainebleau sandstone consists of quartz grains of around $200\mu\text{m}$ in diameter, with porosities ranging from 3% to 30% due to quartz cementation. It has small quantities of clay, is considered water wet and surface conductance is considered negligible. As this data set

contains plugs which share geological history, it is expected to have a correlation between the geometrical factor and porosity.

In Fig. 6(a), we have plotted the geometrical factor E_0 versus porosity ϕ , while the formation conductivity factor f versus porosity ϕ are plotted in Fig. 6(b). Figure 6(b) also contains a fit to a power law relation, as suggested by Bruggeman and Archie (Bruggeman, 1935; Archie, 1942). The resulting power law relation $f(\phi) = 0.599\phi^{1.516}$ leads to a coefficient of determination of 0.948. We observe that the simple linear fit $f(\phi) = 0.374\phi + 0.020$, also included in Fig. 6(b), gives a slightly better fit of 0.959 using the same number of adjustable parameters. Other functional relationships with the same number of adjustable parameters are expected to give similar fit to this data.

The plot between the geometrical factor E_0 versus porosity ϕ in Fig. 6(a) contains the same information as the plot in Fig. 6(b), it is just a transformation employing the equality $f = E_0 \phi$. Any functional relationship between porosity and formation conductivity factor would lead to a functional relationship between porosity and the geometrical factor through this transformation. As the transformation is non-linear, the transformed functional relationships will no longer be the best fit to the data. In Fig. 6(a), we have included best fits of the transformed functional relationships used in Fig. 6(b). We observe that the resulting coefficient of determinations indicate that the power-law gives a slightly better fit than the transformed linear function, which is inverted from the case in Fig. 6(b).

Despite the shared geological history for our Fontainebleau samples, the scatter in the data in Fig. 6(a) precludes any definite conclusion about the best correlation

to describe the geometric factor-porosity relationship. This helps to explain the high number of different correlation models in the literature (see Ghanbarian *et al.* (2013a) for an overview of different models). A scatter of this sort implies that the sample suite is somewhat heterogeneous; that is, the samples experienced differences in their geologic evolution in addition to varying degrees of a single formative geologic process which relates them. Explaining this scatter by measurement error is ruled out based on relative small variation in results when repeating resistivity measurements (McPhee *et al.*, 2015).

Notwithstanding the lack of a clear relation between the pore structure and porosity for the Fontainebleau sample set, possible relations arising from a shared geological rock forming process might be lost in the transformation to the formation conductivity factor versus porosity. This is evident when comparing the curve fits in Fig. 6, where the best functional relationship is changed under this transformation. Further, the non-linear transformation given by $f = E_0 \phi$ reduce the scatter in formation conductivity factor versus porosity relative to the scatter in geometrical factor versus porosity. The high coefficients of determination for functional relationships linking the formation conductivity factor to porosity, as seen in Fig. 6(b), could be misinterpreted as originating from pore structure relations. However, the high coefficients of determination is a result of the non-linear transformation, as evident from Fig. 6. Such formation conductivity factor versus porosity plots are not highlighting any underlying correlation, quite the contrary, they obscure any underlying correlation between the pore space geometry and the porosity.

The better fit for the linear relation in Fig. 6(b) could possibly be attributed to the threshold porosity introduced by this function. An explanation for the occurrence of such a percolation threshold for the Fontainebleau material will be given in the next section. Percolation theory has been widely used to describe transport properties of porous materials, such as rock and soil samples (Berkowitz & Balberg, 1993; Mavko & Nur, 1997; Ghanbarian *et al.*, 2013b; Ghanbarian & Berg, 2017). The pore space becomes disconnected at low porosities, and the minimum porosity for a connected pore space is called the percolation threshold porosity ϕ_c . Critical exponents can describe transport properties when the porosity is close to the percolation threshold, but the validity further away from the threshold is unclear. The applicability of percolation theory is further limited by the spread in transport properties for similar porosity values. Still, both plots in Fig. 6 indicate a percolation threshold, with the linear correlation $f(\phi) = 0.374(\phi - \phi_c)$ in Fig. 6(b) giving a percolation threshold of

$\phi_c = 0.020/0.374 = 0.0535$, while the corresponding correlation in Fig. 6(a) gives $\phi_c = 0.016/0.337 = 0.0475$.

DESCRIPTION OF THE GEOMETRICAL FACTOR

Advances in imaging have made it possible for direct imaging of the pore structure in reservoir rocks with a resolution that allows for direct computation of electrical conductivity with a high degree of accuracy. In combination with modelling of rock-forming processes, this opens new possibilities for understanding the features controlling electrical conductivity and transport in porous media in general.

Saturated porous media with varying porosity

To investigate the relation between pore structure and conductivity, we consider seven digital rock models of the Fontainebleau sandstone, generated with the e-Core software (Berg, 2014). Identical grain size distribution, sedimentation, compaction and diagenetic process parameters for the model constructions were used. Porosity values between 8% and 25% were obtained by varying only the amount of quartz cementation. These models could therefore help to investigate the effect of quartz cementation, while all other parameters are kept constant.

On the grid representation of our three-dimensional models, we introduced an electrical potential $\Delta\Phi$ over two opposite end-planes of the sample and numerically solved the three-dimensional Laplace equation $\nabla^2\Phi = 0$ by a finite difference method to obtain the potential field Φ everywhere in the pore space. The potential field for the sample with 21% porosity is visualized in Fig. 7. On the resulting electric field $E = -\nabla\Phi$, we tracked electric field lines, and calculated the tortuosity and constriction factor as given by the Equations (20) and (22) introduced above. More information on the numerical solutions and field line tracking methods can be found in Berg and Held (2016). The resulting tortuosity and constriction factor values are plotted in Fig. 8. The reason for plotting the inverse values in Fig. 8(a), is that this is the way they occur in the expression for the geometrical factor: $E_0 = \tau^{-2} C^{-1}$. We have also included two curve fits in Fig. 8(a) to indicate the evolution of the two pore structure parameters with respect to the modelled quartz cementation process. The functions used for these curve fits have no physical interpretations.

Observe in Fig. 8(a) that the trend of the inverse constriction factor crosses the x -axis at a positive porosity value. This indicates a possible percolation threshold for the porosity at

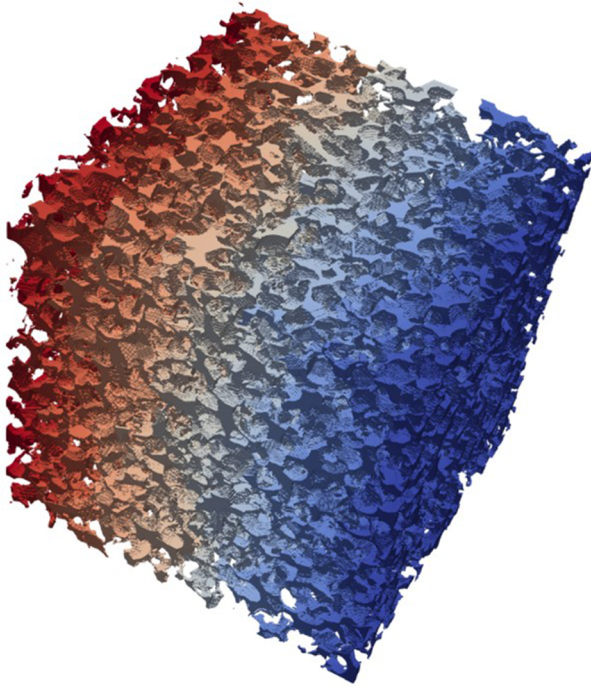


Figure 7 The 3D pore structure of the Fontainebleau sample with approximately 21% porosity, where the solution of the Laplace equation is indicated by the colours.

the vanishing constriction factor. The trend for the tortuosity values indicates a positive value at the apparent percolation threshold given by the constriction factor. This positive tortuosity value at the percolation threshold indicates that the tortuosity is not determined by the connectivity of the pore space. The origin for the percolation threshold is thus the constriction factor alone, and not the tortuosity.

The calculated geometrical factor $E_0 = \tau^{-2} C^{-1}$ is plotted versus porosity in Fig. 9, together with two sets of experimental data; the already introduced data set from (Jacquin, 1964) and an additional dataset from (Gomez *et al.*, 2010). We have also plotted the product of the two trend lines in Fig. 8 as the dashed curve in Fig. 9. The combined curves given by the dashed line exhibit a non-trivial shape roughly similar to the trend suggested by the observed data. This dashed curve indicates a percolation threshold for the geometrical factor, being the porosity value where the constriction factor goes to zero. Note that this percolation threshold is the threshold for the considered grain pack under increasing quartz cementation, and not for the Fontainebleau material in general. The Fontainebleau material will exhibit a larger spread in transport properties, complicating the use of a single percolation

threshold as it occurs for the modelled rock-forming process with changes in the amount of cementation only.

We observe a large spread in the experimental data compared to the trend of our calculated data. As the digital rock models were created by changing only one parameter in the rock forming process, namely the amount of quartz cementation, it is as expected that their effective values follow a clear trend. The experimental data on the other hand contains rocks with varying grain size distribution, sorting, etc., all of which creates a larger spread when plotted versus porosity. Still, as the Fontainebleau rock type is characterized by well-sorted grains with varying degrees of quartz cementation, it is expected that the modelled and experimental data should follow the same trend. Inspection of Fig. 9 suggests that it does.

Partially saturated porous media

We will now investigate the changes in geometrical descriptors for a partially saturated sample. For this investigation, we avoided the lower porosity values, as we did not want a sample close to the percolation threshold. We therefore chose the Fontainebleau sample with approximately 25% porosity. As we need high resolution for our water phase to be able to calculate good approximations for the geometrical descriptors, we chose to employ a network simulation where the fluid distribution is dictated by capillary forces (Ramstad *et al.*, 2019). Hence, we neglect viscous forces, while gravitational forces are negligible at the given sample size. The e-Core software was used both to generate the network and to simulate primary drainage. The network applied is shown in Fig. 10.

The primary drainage is simulated by a quasi-static process, where we increase the capillary pressure step-wise, and for each capillary pressure step calculate which pores are invaded by an invasion percolation algorithm (Bakke & Øren, 1997; Blunt, 2017). For each saturation step, we calculated the geometrical descriptors $\tau_t(S_w)$ and $C_t(S_w)$ using a field line tracing method similar to Berg (2012) and Torland (2018). The fractional values given by the tortuosity index $\tau_i = \tau_t / \tau_0$ and constriction index $C_i = C_t / C_0$ are plotted in Figs 11 and 13. The plot of the tortuosity index reveals a relatively small change in tortuosity for the whole saturation range. Thus, also for lower saturations, the main influence for the tortuosity is the underlying pore structure. This suggests that the water phase is well connected even for lower saturations.

The tortuosity index in Fig. 11 shows a non-trivial behaviour, where for decreasing saturation it first increases, then drops, before increasing again. During primary drainage, the non-conductive phase will fill the bulk of the pores, leaving

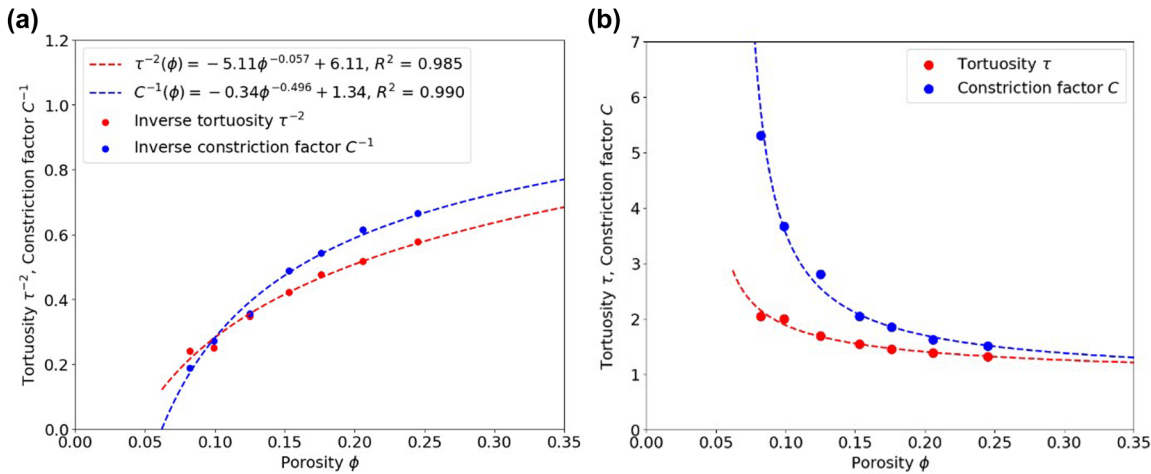


Figure 8 Plot of the calculated values for a) inverse tortuosity squared and the inverse constriction factor versus porosity, together with two curve fits, and b) tortuosity and constriction factor.

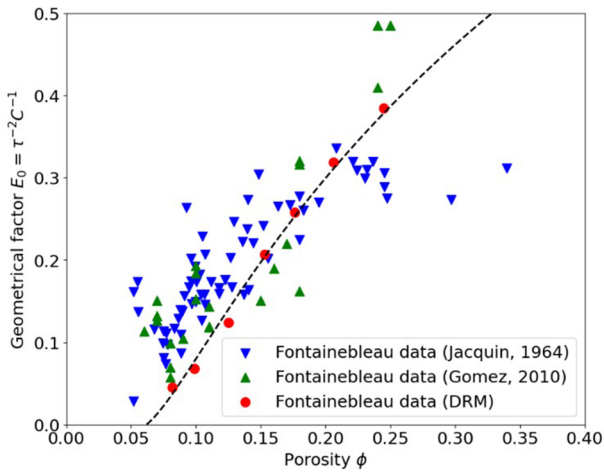


Figure 9 Plot of geometrical factor versus porosity for two sets of experimental data and for our digital rock models. The dashed line gives the product of the two curves plotted in Fig. 8, indicating a trend for the digital rock models.

the conductive brine to reside as films on the rock surface. During the first part of the drainage process, this will yield a mixture of pores fully occupied by brine and pores where the brine only resides as films. It is expected that this mixture of film and bulk conductance increases the length of the field lines, thereby increasing the tortuosity index, as illustrated in Fig. 12(b). At lower saturations, most pores will be filled with the non-conductive phase, with the conductive brine left residing in films. In this situation, the relative difference in conductance between the individual pores is expected to have a distribution similar to the fully saturated case, albeit at a lower absolute value. This will reduce the length of the field lines to-

wards values seen in the fully saturated sample, and is assumed to account for the reduction in tortuosity index. This is illustrated by Fig. 12(a) and (c), representing the fully saturated and the situation where the bulk phase has been replaced by the non-conductive phase. In this illustration, the field lines have comparable lengths. At very low saturations, the brine films start to rupture, leading to a second increase in tortuosity index.

The constriction factor plotted in Fig. 13 is changing more than an order of magnitude for the given saturation change. Thus, the change in constriction factor is much larger than the change in the tortuosity. This indicates that the saturation change induces a relatively large change in brine cross-sectional area in the pores. Although the absolute reduction in pore throat brine volume might be in the same range as the absolute change in water volume in the pore bodies, the change in the brine cross-sectional area in the pore throats has a much larger impact on the overall conductivity through the brine phase.

For most of the saturation range, the changes in the tortuosity factor are smaller than 10%, while the constriction factor changes with more than an order of magnitude. This indicates that the change in geometrical structure that matters is the variation in the constriction factor. This observation is clearly illustrated in Fig. 14. By omitting the tortuosity index, we observe that the resistivity index is well approximated by the constriction factor index and saturation alone. The fitted saturation exponent is -1.98 when we include the tortuosity, while it is -1.88 when the tortuosity is omitted. In contrast, omitting the constriction factor would have changed the fitted saturation exponent radically. Thus, what is

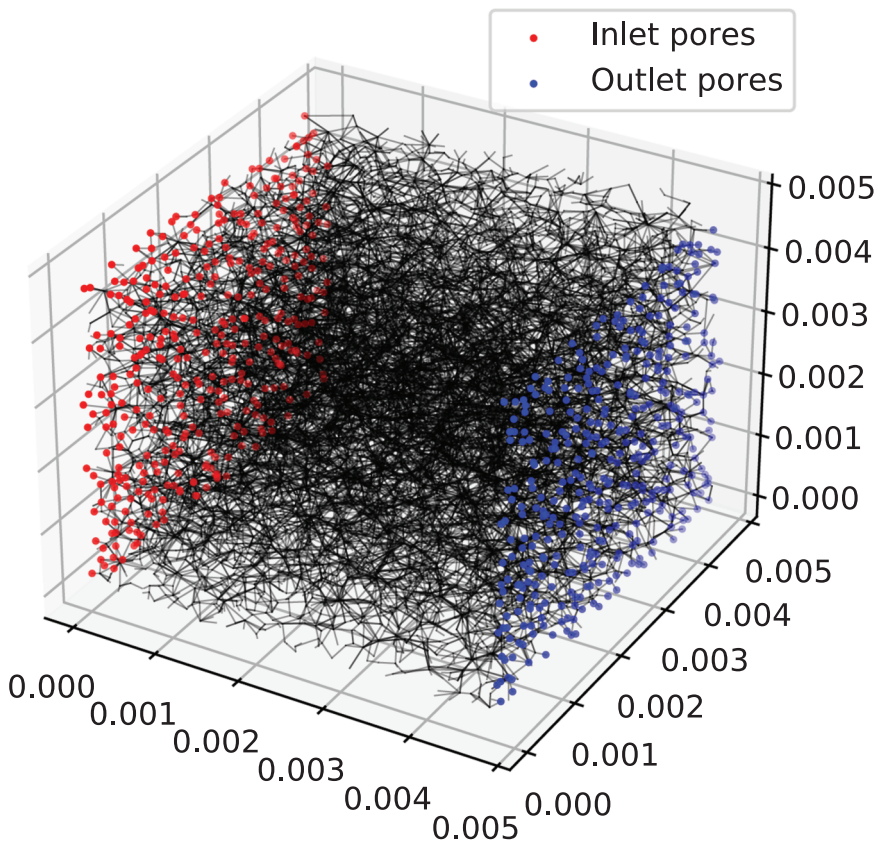


Figure 10 The extracted pore network from the Fontainebleau sample with approximately 25% porosity. The inlet and outlet nodes are indicated by red and blue dots, respectively.

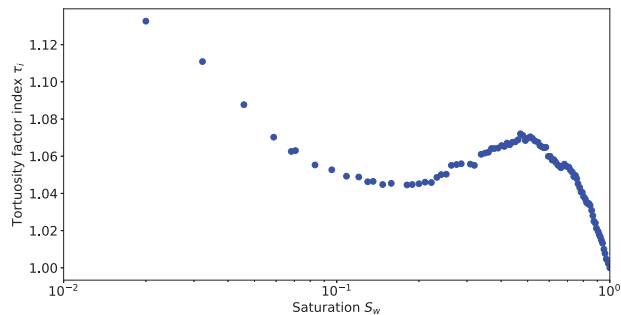


Figure 11 The tortuosity index $\tau_t = \tau_t / \tau_0$ calculated for different saturations during primary drainage in our Fontainebleau sample with 25% porosity.

important for describing the resistivity index is the constriction factor index. Given the nearly exclusive focus on tortuosity in the literature, this result might surprise some readers.

CONCLUSION

In this article, we consider the problem of characterizing the effective conductivity in partially saturated porous media

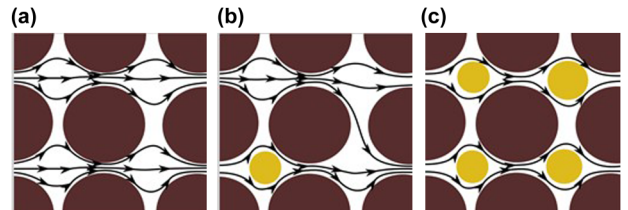


Figure 12 A cartoon illustrating the change in tortuosity at different saturations. The brown circles are idealized non-conductive grains, the orange represents the imbibing non-conductive phase, while white is the electrolyte. The lines illustrate the electrical field lines. In (a) the sample is fully saturated by the electrolyte, in (b) it is partially saturated, while in (c) it is close to the residual electrolyte saturation, where the wetting electrolyte resides as films covering the solid surface.

based on a description of the electrolyte geometry. The authors have previously introduced a complete first principles-based description of conductivity in porous media. A geometrical factor E_0 has been introduced which, together with porosity ϕ and electrolyte conductivity σ_w , describes the conductivity σ_0 of a saturated porous medium as $\sigma_0 = \sigma_w \phi E_0$. This geometrical factor was separated into two intrinsic geometrical

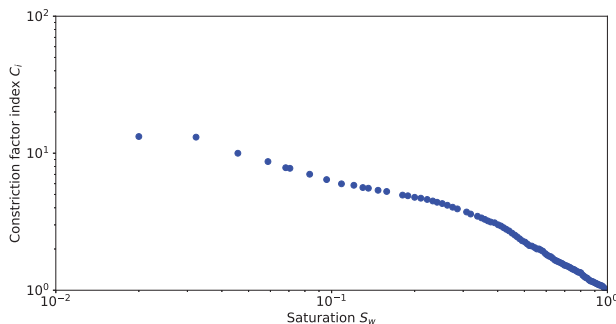


Figure 13 The constriction factor index $C_i = C_t / C_0$ calculated for different saturations during primary drainage in our Fontainebleau sample with 25% porosity.

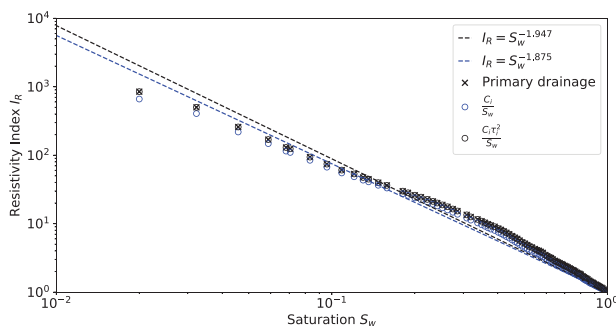


Figure 14 The resistivity index I_R for primary drainage, compared to the resistivity index obtained from the pore structure indices tortuosity index and constriction factor index. The black crosses indicate the resistivity index as calculated from the overall conductance. The black circles are the resistivity index calculated from the constriction index and tortuosity index, and additionally the saturation. The black circles and black crosses fall on top of each other, as predicted by Equation (27). The blue circles indicate the resistivity index as predicted by the saturation and constriction factor index only, neglecting tortuosity, thereby illustrating its relatively minor influence.

descriptors accounting for the tortuosity τ and constriction C of the pore space geometry, with their product describing the geometrical factor as $E_0 = 1/(\tau^2 C)$.

In partially saturated porous media, or multi-phase situations, the connected conductive fluid phase undergoes changes in geometry. These geometry changes induce changes in conductivity, traditionally represented by the resistivity index. In this article, the geometrical description for fully saturated porous media, $E_0 = 1/(\tau^2 C)$, has been extended to partially saturated porous media, where the structure of the water phase at different saturations is described by the same pore structure parameters. By defining the relative change in pore structure parameters as a tortuosity index τ_i and constriction factor index C_i , we have shown that the resistivity index can

be described as $I_R = \tau_i^2 C_i / S_w$. These indices characterize the change in geometry and its effect on the conductivity. Both single and multiphase conductance descriptions are illustrated using three-dimensional pore space models and simulated fluid distributions. Numerical simulation of primary drainage in a model of a Fontainebleau sample indicated that the controlling factor for the resistivity index is the change in constriction factor, while the changes in tortuosity played a minor role. Additionally, the simulated fluid distributions exposed non-trivial changes in fluid geometry which are masked by the traditional description using a resistivity index. This exemplifies how our introduced conductance description through porosity, saturation and a geometrical factor, decomposed into separate terms accounting for tortuosity and constrictivity, opens up new insights and understanding of conductance and bulk conductivity of porous media.

ACKNOWLEDGEMENTS

The first author was supported by the Research Council of Norway through its Centers of Excellence funding scheme, project number 262644, PoreLab.

DATA AVAILABILITY STATEMENT

The digital rock models of Fontainebleau sandstone used in this study is available in the Digital Rocks Portal at <http://doi.org/10.17612/P75P4P>.

TABLE OF NOTATIONS AND UNITS

This table is constructed as an aid to readers. The base units in this table are mass, length, time, charge (**M**, **L**, **T**, **Q**). We have used charge as a base unit instead of the current SI standard, the ampere (**I**), as it makes the basic physical quantities more clearly understandable. Derivative units can be expressed descriptively in more than one way. For example, resistance can be expressed as ohms, as volts/ampères, or as (Joules/Coulomb)/ampères or (Joules/Coulomb)/(Coulomb/second). In this table, we sometimes supply more than one of the possible choices, enclosed by parenthesis and separated by commas. The base units (where supplied) are introduced by a semicolon and in bold-faced Calibri font. Many ratios are ‘unitless’ but are more clearly expressed when the units of denominator and numerator are shown. For example, porosity is the ratio of two volumes. These are explicitly expressed.

a	Archie model parameter; so-called ‘tortuosity’ factor, (unitless)	m	Archie model parameter, porosity exponent, so-called ‘cementation’ exponent, (unitless)
A	cross-sectional area of sample volume, (area), (length ²); (L ²)	n	Archie model parameter, saturation exponent, (unitless)
A'	void cross-sectional area of sample, (area), (length ²); (L ²)	P	power, (rate of energy conversion to joule heating of the porous sample), (energy/time); (M L ² T ⁻³)
$A(x)$	cross-sectional area of sample void volume at distance x from the origin, (length ²); (L ²)	R_t	resistance of tube inside porous medium, (Ohm); (M L ² T ⁻¹ Q ⁻²)
A_e	‘effective’ cross-sectional area of sample void volume, (length ²); (L ²)	$dR_t(x)$	resistance of the tube cross-section of width dx at distance x from the origin, (Ohm-meter); (M L ² T ⁻¹ Q ⁻²)
\bar{A}	average cross-sectional area of sample void volume, (length ²); (L ²)	s	field line (or arc) length along the field line S , (length); (L)
C	constriction factor, defined by Equation (17), (area/area); (L ² /L ²)	S	field line described by the intersection of the two surfaces given by λ and χ
C_0	constriction factor in fully saturated pore space, (unitless)	S_w	water saturation, (volume/volume); (L ³ /L ³)
C_t	constriction factor in partially saturated pore space, (unitless)	V	sample volume, (length ³); (L ³)
C_i	constriction index, $C_i = C_t / C_0$, (unitless)	x	coordinate in direction of applied potential and electric field, (length); (L)
e_i	efficiency index, E_t/E_0 , (unitless)	y, z	coordinates orthogonal to applied potential and electric field, (length); (L)
e_t	efficiency index as denoted in Herrick and Kennedy (2009)	Γ	the curved path of an electric field line traversing the sample (length); (L)
E	electrostatic field, $E = -\nabla\Phi$, (volt/m), (Joule/Coulomb/meter); (M L T ² Q ⁻¹)	λ	coordinate for surface containing electric field line, (L)
E'	electric field along path L' , (volt/m)	Λ	function from Cartesian coordinates to a scalar field
E_t	geometrical factor for partially saturated pore space, (unitless)	ρ_0	effective fully saturated porous medium resistivity, (Ohm-meter), (volt/ampere-meter)
E_0	geometrical factor for saturated pore space, (unitless)	ρ_t	effective (partially saturated) porous medium resistivity, (Ohm-meter), (volt/ampere-meter)
f	formation conductivity factor, $f = 1/F$, (conductivity/conductivity)	ρ_w	electrolyte (brine) resistivity, (Ohm-meter)
F	formation resistivity factor, (resistivity/resistivity)	σ	conductivity, Siemens/meter, (amperes/volt/meter); (M ⁻¹ L ⁻³ T Q ²)
I	electric current (current density integrated over area) through the sample, (ampere); (Q/T)	σ_0	conductivity of sample fully saturated with the electrolyte, $\sigma_0 = 1/R_0$, (Siemens/meter)
I_R	resistivity index, (resistivity/resistivity)	σ_t	conductivity of sample partially saturated with the electrolyte, $\sigma_t = 1/R_0$, (Siemens/meter)
I_Γ	current carried by the streamtube spanned by $d\lambda d\chi$, (amperes); (Q/T)	σ_w	electrolyte (brine) conductivity, (Siemens/meter)
J	Jacobian, (length/length)	τ	tortuosity, $\tau = L' / L$ for single channel, given by Equation (15) for complex porous medium, (length/length); (L/L)
J	interstitial current density, (ampere/meter ² ; coulomb/sec/meter ²); (L ⁻² T ⁻¹ Q)	τ_0	tortuosity in saturated sample, (length/length)
J_0	effective current density, (ampere/meter ²)	τ_t	tortuosity in partially saturated sample, (length/length)
J_x	component of interstitial current density in x direction, (ampere/meter ²)	τ_i	tortuosity index, $\tau_i = \tau_t / \tau_0$, (unitless)
J'	current density along path L' , (ampere/meter ²)	ϕ	porosity, $\phi = \Omega/V$, (volume/volume); (L ³ /L ³)
L	length of sample, (meters); (L)	Φ	electric potential, (volts; joule/coulomb); (M L ² T ⁻² Q ⁻¹)
L'	length of tortuous pore channel through sample, (meters)		
L_Γ	length of electric field line Γ through sample, (meters)		

$\Delta\Phi$	potential difference (or voltage) across sample, (volts)
$\nabla\Phi$	gradient of applied electric potential, $-\nabla\Phi = \mathbf{E}$ (volt/meter), (joule/coulomb/meter); ($\mathbf{M} \, \mathbf{L} \, \mathbf{T}^{-1} \, \mathbf{Q}^{-1}$)
$\nabla^2\Phi$	Laplacian of electrical potential, charge density/permittivity; ($\mathbf{M} \, \mathbf{T}^{-2} \, \mathbf{Q}^{-1}$)
χ	coordinate for surface containing an electric field line, (L)
X	function from Cartesian coordinates to a scalar field
Ω	subspace given by the electrolyte (the void volume for a fully saturated sample), (length ³); (\mathbf{L}^3)

ORCID

Carl Fredrik Berg 

<https://orcid.org/0000-0002-9223-8715>

REFERENCES

- Archie, G.E. (1942) The electrical resistivity log as an aid in determining some reservoir characteristics. *Transactions of the AIME*, 146, 54–62.
- Bakke, S. & Øren, P.-E. (1997) 3-D pore-scale modelling of sandstones and flow simulations in the pore networks. *SPE Journal*, 2, 136–149.
- Bear, J. (1988) *Dynamics of fluids in porous media*. Downers Grove, IL: Dover.
- Berg, C.F. (2012) Re-examining Archie's law: Conductance description by tortuosity and constriction. *Physical Review E*, 86, 046314.
- Berg, C.F. (2014) Permeability description by characteristic length, tortuosity, constriction and porosity. *Transport in Porous Media*, 103, 381–400.
- Berg, C.F. & Held, R. (2016) Fundamental transport property relations in porous media incorporating detailed pore structure description. *Transport in Porous Media*, 112, 467–487.
- Berkowitz, B. & Balberg, I. (1993) Percolation theory and its application to groundwater hydrology. *Water Resources Research*, 29, 775–794.
- Blunt, M.J. (2017) *Multiphase flow in permeable media: a pore-scale perspective*. Cambridge: Cambridge University Press.
- Boyack, J.R. & Giddings, J.C. (1963) Theory of electrophoretic mobility in stabilized media. *Archives of Biochemistry and Biophysics*, 100, 16–25.
- Bruggeman, V.D. (1935) Berechnung verschiedener physikalischer Konstanten von heterogenen Substanzen. I. Dielektrizitätskonstanten und Leitfähigkeiten der Mischkörper aus isotropen Substanzen. *Annals of Physics*, 416, 636–664.
- Cai, J., Wei, W., Hu, X. & Wood, D.A. (2017) Electrical conductivity models in saturated porous media: a review. *Earth-Science Reviews*, 171, 419–433.
- Carman, P.C. (1937) Fluid flow through granular beds. *Transactions of the Institution of Chemical Engineers*, 15, 150–166.
- Clennell, M.B. (1997) Tortuosity: a guide through the maze. *Geological Society, London, Special Publications*, 122, 299–344.
- Cornell, D. & Katz, D.L. (1953) Flow of gases through consolidated porous media. *Industrial & Engineering Chemistry Research*, 45, 2145–2152.
- Currie, J.A. (1960) Gaseous diffusion in porous media. Part 2. Dry granular materials. *British Journal of Applied Physics*, 11, 318.
- Dullien, F.A. (1992) *Porous media: fluid transport and pore structure*. Cambridge, MA: Academic Press.
- Dullien, F.A.L. (1975) Prediction of "tortuosity factors" from pore structure data. *Aiche Journal*, 21, 820–822.
- Duy Thanh, L., Jougnot, D., Van Do, P. & Van Nghia, A, N. (2019) A physically based model for the electrical conductivity of water-saturated porous media. *Geophysical Journal International*, 219, 866–876.
- Ellis, D.V. & Singer, J.M. (2007) *Well logging for earth scientists*. Berlin: Springer.
- Fatt, I. (1956) The network model of porous media. *Transactions of the AIME*, 207, 144–181.
- Ghanbarian, B. & Berg, C.F. (2017) Formation factor in Bentheimer and Fontainebleau sandstones: theory compared with pore-scale numerical simulations. *Advances in Water Resources*, 107, 139–146.
- Ghanbarian, B., Hunt, A.G., Ewing, R.P. & Sahimi, M. (2013a) Tortuosity in porous media: a critical review. *Soil Science Society of America Journal*, 77, 1461–1477.
- Ghanbarian, B., Hunt, A.G., Sahimi, M., Ewing, R.P. & Skinner, T.E. (2013b) Percolation theory generates a physically based description of tortuosity in saturated and unsaturated porous media. *Soil Science Society of America Journal*, 77, 1920–1929.
- Glover, P. (2009) What is the cementation exponent? A new interpretation. *The Leading Edge*, 28, 82–85.
- Gomez, C.T., Dvorkin, J. & Vanorio, T. (2010) Laboratory measurements of porosity, permeability, resistivity, and velocity on Fontainebleau sandstones laboratory measurements on sandstones. *Geophysics*, 75, E191–E204.
- Guyod, H. (1944) Fundamental data for the interpretation of electric logs, Part 12. *Oil Weekly*, 115, 72–77.
- Hanai, T. (1968) Electrical properties of emulsions. *Emulsion Science*.
- Herrick, D.C. (1988) *Conductivity models, pore geometry, and conduction mechanisms*. SPWLA 29th Annual Logging Symposium. Society of Petrophysicists and Well-Log Analysts.
- Herrick, D.C. & Kennedy, W.D. (2009) *A new look at electrical conduction in porous media: a physical description of rock conductivity*. SPWLA 50th Annual Logging Symposium. Society of Petrophysicists and Well-Log Analysts.
- Herrick, D.C. & Kennedy, W.D. (1994) Electrical efficiency—a pore geometric theory for interpreting the electrical properties of reservoir rocks. *Geophysics*, 59, 918–927.
- Holzer, L., Wiedenmann, D., Münch, B., Keller, L., Prestat, M., Gasser, P. et al. (2013) The influence of constrictivity on the effective trans-

- port properties of porous layers in electrolysis and fuel cells. *Journal of Materials Science*, 48, 2934–2952.
- Jacquin, C.G. (1964) Corrélation entre la perméabilité et les caractéristiques géométriques du grès de Fontainebleau. *Revue de l'Institut Francais du Petrole*, 19, 921.
- Jakosky, J.J. & Hopper, R.H. (1937) The effect of moisture on the direct current resistivities of oil sands and rocks. *Geophysics*, 2, 33–54.
- Johnson, D.L., Koplik, J. & Schwartz, L.M. (1986) New pore-size parameter characterizing transport in porous media. *Physical Review Letters*, 57, 2564.
- Katz, A. & Thompson, A.H. (1985) Fractal sandstone pores: implications for conductivity and pore formation. *Physical Review Letters*, 54, 1325.
- Kennedy, W.D. & Herrick, D.C. (2012) Conductivity models for Archie rocks. *Geophysics*, 77, WA109–WA128.
- Kennedy, W.D., Herrick, D.C. & Yao, T. (2001) Calculating water saturation in electrically anisotropic media. *Petrophysics* 42, 118–136.
- Knackstedt, M.A. & Zhang, X. (1994) Direct evaluation of length scales and structural parameters associated with flow in porous media. *Physical Review E*, 50, 2134.
- Koponen, A., Kataja, M. & Timonen, J. (1997) Permeability and effective porosity of porous media. *Physical Review E*, 56, 3319.
- Kozeny, J. (1927) Über kapillare Leitung des Wassers im Boden: (Aufstieg, Versickerung und Anwendung auf die Bewässerung). Hölder-Pichler-Tempsky.
- Leverett, M.C. (1938) Flow of oil-water mixtures through unconsolidated sands. *Transactions of the AIME*, 132, 149–171.
- Martin, M., Murray, G.H. & Gillingham, W.J. (1938) Determination of the potential productivity of oil-bearing formations by resistivity measurements. *Geophysics*, 3, 258–272.
- Matyka, M., Khalili, A. & Koza, Z. (2008) Tortuosity-porosity relation in porous media flow. *Physical Review E*, 78, 026306.
- Mavko, G. & Nur, A. (1997) The effect of a percolation threshold in the Kozeny-Carman relation. *Geophysics*, 62, 1480–1482.
- Maxwell, J.C. (1873) *A treatise on electricity and magnetism*. Oxford: Macmillan and Co.
- McPhee, C., Reed, J. & Zubizarreta, I. (2015) *Core analysis: a best practice guide*. Amsterdam: Elsevier.
- Monaro, B. & Han, M. (2009) A connectivity model for the electrical conductivity of sandstone rocks. SPWLA 50th Annual Logging Symposium. Society of Petrophysicists and Well-Log Analysts.
- Owen, J.E. (1952) The resistivity of a fluid-filled porous body. *Journal of Petroleum Technology*, 4, 169–174.
- Petersen, E.E. (1958) Diffusion in a pore of varying cross section. *Aiche Journal*, 4, 343–345.
- Pfannkuch, H.-O. (1972) On the correlation of electrical conductivity properties of porous systems with viscous flow transport coefficients. *Developments in Soil Science*, 2, 42–54.
- Pride, S. (1994) Governing equations for the coupled electromagnetics and acoustics of porous media. *Physical Review B*, 50, 15678.
- Ramstad, T., Berg, C.F. & Thompson, K. (2019) Pore-scale simulations of single-and two-phase flow in porous media: approaches and applications. *Transport in Porous Media*, 130, 77–104.
- Rembert, F., Jougnot, D. & Guaracino, L. (2020) A fractal model for the electrical conductivity of water-saturated porous media during mineral precipitation-dissolution processes. *Advances in Water Resources*, 145, 103742.
- Revil, A. & Glover, P.W.J. (1997) Theory of ionic-surface electrical conduction in porous media. *Physical Review B*, 55, 1757.
- Schopper, J.R. (1966) A theoretical investigation on the formation factor/permeability/porosity relationship using a network model. *Geophysical Prospecting*, 14, 301–341.
- Sen, P.N., Scala, C. & Cohen, M.H. (1981) A self-similar model for sedimentary rocks with application to the dielectric constant of fused glass beads. *Geophysics*, 46, 781–795.
- Slawinski, A. (1926) Conductibilité d'un électrolyte contenant des sphères dielectriques. *Journal of Chemical Physics*, 23, 710–727.
- Tiab, D. & Donaldson, E.C. (2015) *Petrophysics: theory and practice of measuring reservoir rock and fluid transport properties*. Houston, TX: Gulf Professional Publishing.
- Tjaden, B., Cooper, S.J., Brett, D.J., Kramer, D. & Shearing, P.R. (2016) On the origin and application of the Bruggeman correlation for analysing transport phenomena in electrochemical systems. *Current Opinion in Chemical Engineering*, 12, 44–51.
- Torland, A. (2018) *A pore network investigation of factors influencing the residual oil saturation*. Master's Thesis, NTNU.
- Van Brakel, J. & Heertjes, P.M. (1974) Analysis of diffusion in macro-porous media in terms of a porosity, a tortuosity and a constrictivity factor. *International Journal of Heat & Mass Transfer*, 17, 1093–1103.
- Waxman, M.H. & Smits, L.J.M. (1968) Electrical conductivities in oil-bearing shaly sands. *Society of Petroleum Engineers Journal*, 8, 107–122.
- Wheatcraft, S.W. & Tyler, S.W. (1988) An explanation of scale-dependent dispersivity in heterogeneous aquifers using concepts of fractal geometry. *Water Resources Research*, 24, 566–578.
- Winsauer, W.O., Shearin Jr, H.M., Masson, P.H. & Williams, M. (1952) Resistivity of brine-saturated sands in relation to pore geometry. *Aapg Bulletin*, 36, 253–277.
- Wyckoff, R.D. & Botset, H.G. (1936) The flow of gas-liquid mixtures through unconsolidated sands. *Physics*, 7, 325–345.
- Wyllie, M.R.J. & Rose, W.D. (1950) Some theoretical considerations related to the quantitative evaluation of the physical characteristics of reservoir rock from electrical log data. *Journal of Petroleum Technology*, 2, 105–118.
- Yu, B. & Cheng, P. (2002) A fractal permeability model for bi-dispersed porous media. *International Journal of Heat & Mass Transfer*, 45, 2983–2993.

APPENDIX

Deriving Equation (9)

The Archie model can be succinctly stated as the product of formation resistivity factor F and resistivity index I_R , thus

$$FI_R = \frac{\rho_0}{\rho_w} \frac{\rho_t}{\rho_0} = \frac{\rho_t}{\rho_w}. \quad (\text{A1})$$

When empirical relationships between F and porosity and I_R and brine saturation are substituted, then the familiar form

of the Archie model emerges. However, for almost all theoretical purposes, it is advantageous to use conductivity in the formulation of these relationships. For a homogeneous, isotropic sample shaped as a cylinder with length L and cross-sectional area A , the basic relationship among applied voltage difference $\Delta\Phi$, induced current I , material conductivity σ_t , and material geometry is

$$\frac{I}{\Delta\Phi} = \sigma_t \frac{A}{L} \equiv g, \quad (\text{A2})$$

where the ratio of current to applied voltage is defined as ‘conductance’ and denoted as g . All quantities except the bulk conductivity are directly measurable, so bulk conductivity of the material is determined by $\sigma_t = g L / A$. Thus

$$\sigma_t = \frac{L}{A} \frac{I}{\Delta\Phi}. \quad (\text{A3})$$

and dividing by σ_w with substitution for I from Equation (4) gives

$$\begin{aligned} \frac{\sigma_t}{\sigma_w} &\equiv \frac{1}{\sigma_w} \frac{L}{A} \frac{I}{\Delta\Phi} = \frac{L}{\sigma_w A \Delta\Phi} \left(\frac{1}{\Delta\Phi} \int_{\Omega} \sigma_w \|\nabla\Phi\|^2 dV \right) \\ &= \frac{L}{A \Delta\Phi^2} \int_{\Omega} \|\nabla\Phi\|^2 dV \end{aligned} \quad (\text{A4})$$

Then, noting that for the arbitrary porous medium with total volume V and brine volume Ω , we have $\Omega/V = S_w\phi$. As a final step, multiply the right side of this equation by $1 = L/L$, yielding

$$\begin{aligned} \frac{\sigma_t}{\sigma_w} &= \frac{L}{L} \frac{L}{A \Delta\Phi^2} \int_{\Omega} \|\nabla\Phi\|^2 dV = \frac{1}{V \Delta\Phi/L^2} \int_{\Omega} \|\nabla\Phi\|^2 dV \\ &= S_w\phi \frac{1}{\Omega} \int_{\Omega} \frac{\|\nabla\Phi\|^2}{\Delta\Phi/L^2} dV = S_w\phi E_t \end{aligned} \quad (\text{A5})$$

Term-by-term comparison shows that

$$E_t = \frac{1}{\Omega} \int_{\Omega} \frac{\|\nabla\Phi\|^2}{\Delta\Phi/L^2} dV. \quad (\text{A6})$$

Current density definitions and Equation (7)

Consider a brine-filled sample of length L and cross-sectional area A cut from a porous material. The brine has conductivity σ_w . The cartoon rock sample in Fig. 15 illustrates the grain and pore spaces in the sample. The sample is energized by a potential difference $\Delta\Phi$ applied left-to-right across the sample. Since we can measure both cross-sectional area A and the current I that flows as a result, an effective current density J_0 and conductivity σ_0 for the sample can be computed. Thus, J_0 and σ_0 are not ‘physical’ current density and conductivity

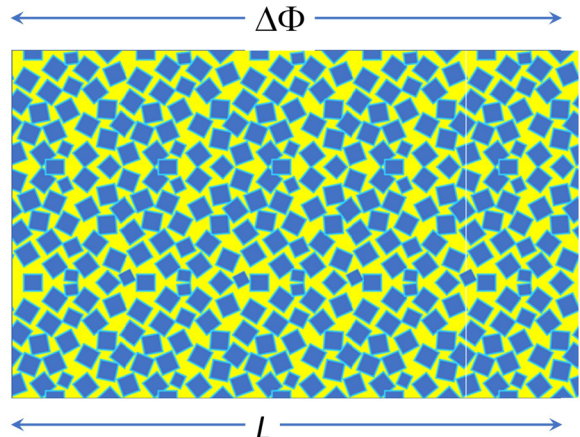


Figure 15 This graphic illustrates pore system of a porous medium. In an Archie rock, the distribution of grains is individually random but homogeneous on the scale of interest. Modelling of a real pore system including every detail is impractical, so the properties of the medium on the scale of interest are the targets for modelling. These properties include average porosity, average conductivity, and average current density, and the relationships among them.

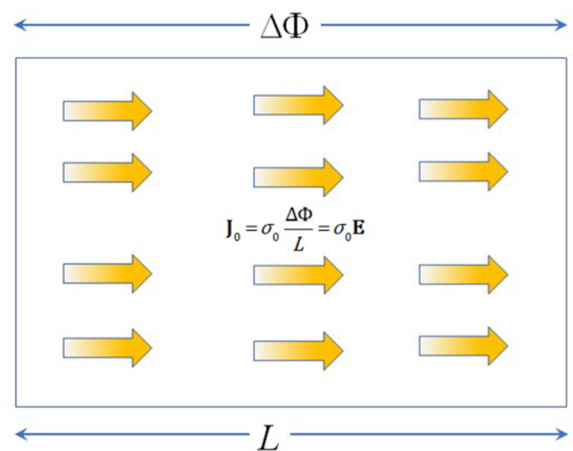


Figure 16 This graphic illustrates the porous medium conceptualized in terms of an ‘effective’ conductivity that is constant and applies to the entire sample volume, and an effective current density which is constant throughout the volume. These are not ‘physical’ parameters since they apply to the bulk volume of the medium, both the conductive and non-conductive phases, and are constant throughout the volume. The actual current density in the medium varies from point-to-point.

since they apply to the entire medium, both the conductive and non-conductive phases, and they are the same at each point in the medium. The actual current density and conductivity in the medium *vary* from point-to-point. Conversely, J_0 and σ_0 are average, or effective, values and are *constant* for all points in the sample, see Fig. 16.

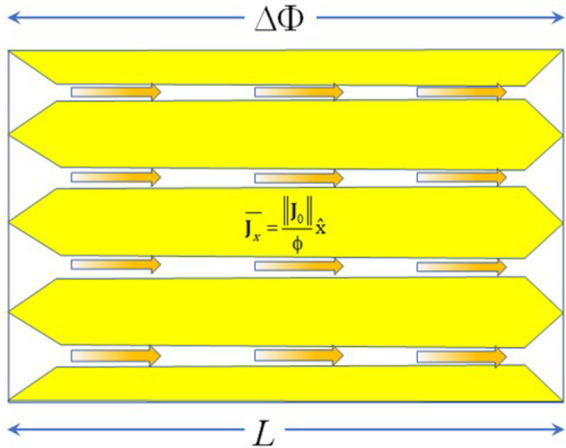


Figure 17 Porosity is taken into account in this average. The total current density J_0 is imagined to flow only in the actual cross-sectional area of voids in the sample. The current density in the void space, imagined as the x component of total current density $\|J_x\|$, is higher than the average current density by a factor $1/\phi$. The \hat{x} is the unit vector in the x direction.

The relationship between current density, bulk conductivity, applied potential, and sample length is $\|J_0\| = \sigma_0 \Delta\Phi/L$. The actual current density in the sample is confined to end-to-end streamtubes, and must be higher than the effective current density. By the definition of current density, the x component must be $\|J_x\| = I/A'$, where A' is the void cross-sectional area normal to x . Dividing I and A' by A leads to $\|J_x\| = \|J_0\|/\phi$, so $\|J_x\| > \|J_0\|$ by a factor of the reciprocal of the porosity fraction. This amounts to a constriction of the area available for current to flow through, as illustrated in Fig. 17. However, modelling the streamtubes as straight-through channels is a simplification. The actual streamtubes will be tortuous, and therefore be longer than L , see Fig. 18. This further restriction results in an even higher current density J in the actual stream-

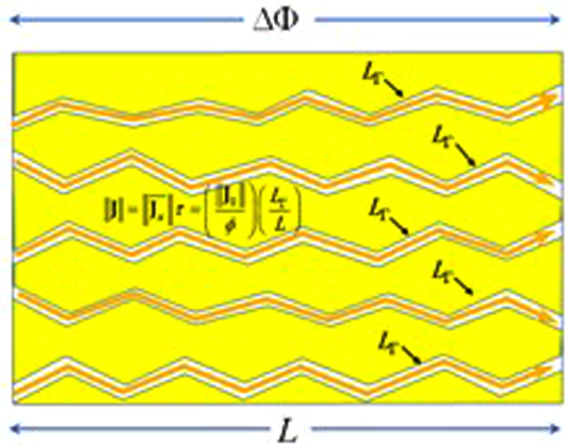


Figure 18 The interstitial current density J , shown as the orange vectors, will be greater than its projection in any direction. Streamtubes of length L_Γ are represented by the zig-zag channels in the model medium. These represent where actual current flows.

tube. This increase in current density will be given by the ratio of the actual streamtube length L_Γ to the end-to-end length L of the sample. Thus,

$$\|J\| = \frac{\|J_0\|}{\phi} \frac{L_\Gamma}{L} = \frac{\|J_0\|}{\phi} \tau = \frac{1}{\phi} \sigma_0 \frac{\Delta\Phi}{L} \frac{L_\Gamma}{L}. \quad (\text{A7})$$

In the streamtubes themselves, J will also obey Ohm's law, or $\|J\| = \sigma_w (\Delta\Phi/L_\Gamma)$. Equating the two formulas for current density gives

$$\sigma_w \frac{\Delta\Phi}{L_\Gamma} = \frac{1}{\phi} \sigma_0 \frac{\Delta\Phi}{L} \frac{L_\Gamma}{L}. \quad (\text{A8})$$

Then, if we combine the terms, we obtain the result

$$\sigma_0 = \sigma_w \phi \left(\frac{L}{L_\Gamma} \right)^2 = \sigma_w \phi \frac{1}{\tau^2} = \sigma_w \phi E_0. \quad (\text{A9})$$